Applied Catalysis B: Environmental 174–175 (2015) 308–322

Contents lists available at ScienceDirect

Applied Catalysis B: Environmental

journal homepage: www.elsevier.com/locate/apcatb

Partial oxidation of methane on Rh/ZrO_2 and $Rh/Ce–ZrO_2$ on monoliths: Catalyst restructuring at reaction conditions

A. Scarabello[a,1], D. Dalle Nogare[b], P. Canu[b], R. Lanza[a,*]

[a] KTH – Royal Institute of Technology, Department of Chemical Engineering and Technology, Teknikringen 42, SE-100 44 Stockholm, Sweden
[b] Department of Industrial Engineering, University of Padua, Via Marzolo 9, 35131 Padova, Italy

ARTICLE INFO

Article history:
Received 15 December 2014
Received in revised form 4 March 2015
Accepted 10 March 2015
Available online 12 March 2015

Keywords:
Methane
Rhodium
Ceria–zirconia
TPR–TPO
Reconstruction

ABSTRACT

0.5% Rh catalysts on ZrO_2 or $CeO_2–ZrO_2$, coated on monoliths were tested for partial oxidation of methane, (GHSV = 100 000 h^{-1}). We ran temperature cycles up to 850 °C, varying the O_2/CH_4 ratio from 0.5 to 0.7. The catalysts were characterized by XRD, TPR/TPO, BET and chemisorption. ZrO_2 required a long conditioning step, to reach stable performance, while the $CeO_2–ZrO_2$ catalyst quickly gained steady activity. The conditioning step is explained with a restructuring of the surface, with the metallic particles becoming smaller. Ceria lowers the ignition temperature by 60 °C. At low temperature, ceria allows an increase in CH_4 conversion and selectivity to syngas. At high temperature, the $CeO_2–ZrO_2$ catalyst significantly increases the CH_4 conversion, compared to ZrO_2, approaching 100%. However, the selectivity to syngas decreases below 80%. The syngas selectivity is higher at lower O_2/CH_4 ratio, at any temperature, but the absolute amount of syngas can be larger with more O_2.

1. Introduction

Catalytic partial oxidation (CPO) of methane has been proposed as an alternative to steam reforming (SR) for the production of syngas [1]. SR is an endothermic process requiring an external heat supply, a furnace in the common industrial practice, usually large for economical convenience. Due to its endothermicity, SR is characterized by a large carbon footprint. On the contrary, CPO is an autothermic process, suitable also for small units that can be assembled together to increase the productivity. Moreover, reactions involved in CPO are more active at process temperature, reducing residence time from seconds, typical of the SR, to milliseconds [2], potentially decreasing reactor volumes by orders of magnitude. Using smaller reactors, yet preserving the same productivity of the large ones, allows using precious metals as catalysts, with the further advantages of reducing the carbon deposition rate and lowering the ignition temperature [3]. Natural gas, which contains up to above 90% of methane, is an increasingly available resource, which is spread around the world in a more homogenous way compared to oil. Furthermore, the proved world reserves are constantly increasing and reached 186 trillion cubic meters in 2014, from about 80 trillion cubic meters in the beginning of the 80's [4]. Biomass gasification is also an increasing source of methane [5], providing a more sustainable alternative. Methane can be simply burned to produce energy, but also represents a good feedstock upgradable to higher value chemicals. By conversion of CH_4 to synthesis gas and subsequent Fischer–Tropsch processes (FT), synthetic, sulfur free fuels can be produced both from biomass and natural gas-derived syngas [6,7]. As a matter of fact, biomass derived fuels, through the so called biomass-to-liquids (BTL) process, represent a very promising source of clean and sustainable fuels for the near future [8]. Beside the aforementioned advantages of CPO over SR, a drawback is related to the different feedstock used. While SR mixes and reacts methane with steam (another energy-consuming factor), in the CPO the co-reagent is air. However, unreacted or excess steam can be removed by condensation, in the low temperature stages of the process, leaving none or little inert (mostly CO_2) in the syngas [9], while air carries a large amount of nitrogen. If syngas is required for the Fischer–Tropsch (FT) synthesis, the dilution with nitrogen is undesirable as the classical industrial process is nitrogen-free, although the $H_2/CO = 2/1$ ratio given by CPO is preferred. However, N_2-rich Fischer–Tropsch processes are possible and might be also economically viable [10]. Further, a nitrogen diluted syngas is suitable for fuel cells applications [11], as well as ammonia and urea syntheses.

Different catalysts have been tested for CPO and the most promising are Rh, Ni, Pd, Pt, Ru, Ir and Co on different supports

* Corresponding author. Tel.: +46 8 790 8281.
E-mail address: lanza@kth.se (R. Lanza).
[1] Present address: Martin Linges vei 33, Fornebu, Norway. Incorporation number: No. 923 609 016 MVA. www.statoil.com.

http://dx.doi.org/10.1016/j.apcatb.2015.03.012
0926-3373/

[12,13]. Ni and Pd decrease their initially high activity in a few hours. Depositions of carbon is relevant (up to 40%), being Ni and Pd quite effective for the Boudouard reaction [14], even though their stability can be improved by tuning the support used [15–18]. Rh-based catalysts show superior H_2 selectivity compared to Pt [19] and are the most promising in methane CPO [7,20].

Alumina has been extensively used as support for many heterogeneous catalysts, including Rh, but may not be the best support. Indeed, as detected in three way catalysts (TWC) Rh can diffuse into the alumina bulk, forming unreactive species, upon exposure to high temperature [21,22]. A solution to this problem came from the use of less reactive supports, such as zirconia (ZrO_2) [23], which showed the highest thermal stability among a number of Rh/metal oxide systems. Zirconia gives stability to catalysts that contain easily reducible rhodium oxide [24,25], and zirconia doped with ceria (CeO_2–ZrO_2) induces significant changes in the activity [26,27]. Besides, it has been proven that the support can enhance the conversion and lower the ignition temperature by enlarging the noble metal dispersion (e.g., ZrO_2) [28] and, with small CeO_2 crystal size, by increasing the O_2 vacancies (e.g., CeO_2–ZrO_2) [29]. If a homogeneous solid solution of ceria–zirconia is obtained, the catalyst shows stable performances under reaction condition, apparently because the increased surface O_2 mobility enhances the carbon release and avoids deposits on the surface [30]. Cited studies report a significant variability, depending on the catalyst dispersion, the particle size of the support and the ratio of CeO_2–ZrO_2, implying that attention must be put on the support selection and preparation, to gain the best performance of the Rh catalyst, due to its active role in the kinetic mechanism [31]. Notwithstanding the large number of publications available on the topic, which is the best support for Rh is still debated [32]. Furthermore, an increasing number of publications have reported rather unclear phenomena of surface reconstruction under reaction conditions, which substantially alter the catalyst performance [28,33–35]. However, the causes of the evolving activity of the catalysts have not been fully clarified, yet. In two recent articles [36,37], Tanaka provides some insights on the issue and discusses restructuring and formation of active sites and reaction intermediates as explanation for the transient behavior detected with some catalysts. Here we report an experimental investigation on CPO with Rh on two supports, ZrO_2 and CeO_2–ZrO_2, washcoated on a monolith, at three fuel-rich stoichiometries and calcined in either oxidizing or reducing atmosphere, highlighting differences in performances both in the conditioning and in the stable operating. The aforementioned differences are related to the structure of the metal particles and the redox properties of the support. Furthermore, a clear activation period is detected for both the supports used and explained in terms of progressive restructuring and reconstruction of the surface, caused by repeated reduction and oxidation cycles under reaction conditions.

2. Experimental

The catalysts tested were prepared with standard incipient wetness techniques and tested in a flow reactor, on a monolith, with a temperature program that cycles heating and cooling several times.

2.1. Catalyst preparation

The catalysts prepared were 0.5 wt% Rh/ZrO_2 and 0.5 wt% Rh/CeO_2–ZrO_2. The support materials used were ZrO_2 (MELCat XZO 631-01) and CeO_2–ZrO_2 (MELCat XZO 802-01, 17.5 wt% CeO_2) supplied by MEL Chemicals. According to the supplier, the CeO_2–ZrO_2 mixture crystallizes forming a solid solution of ceria and zirconia after calcination at 500–550 °C. The Rh precursor was rhodium(III) nitrate solution, 13.97 wt% (Alfa Aesar). The two supporting powders were calcined at 500 °C for 5 h, increasing the temperature with a heating rate of 5 °C/min and cooling at 10 °C/min. Thereafter, the powders were impregnated via incipient wetness, with the nitrate solution. After impregnation, the powders were dried at 110 °C for 1.5 h. Calcination at 800 °C for 4 h concluded the catalyst preparation. To washcoat the monoliths, the calcined powders were mixed with ethanol yielding a slurry, further ball-milled for 24 h. The slurry contained 30 wt% solids and the pH was 8.5 and 7.3 for the zirconia and ceria–zirconia supported sample, respectively. After the ball milling, the slurry appeared stable and homogeneous, but was kept under continuous stirring during dip coating to prevent precipitation. The monolithic material is cordierite (Corning), a highly anisotropic crystalline phase with optimal thermal shock resistance (due to a small thermal expansion), porosity and pore size distribution suitable for washcoating, melting point exceeding 1450 °C, compatibility with washcoat and catalysts, resistance to oxidation. Cordierite monoliths were dipped into the slurry and dried in an oven for 45 min at 110 °C. This procedure was repeated until a catalyst coating of approx. 15 wt% was applied onto the monoliths. The washcoated monoliths were further calcined at 800 °C for 4 h in air to decompose residual salts and consolidate binding to the monolith. Six monoliths were coated with each one of the two catalytic materials prepared, resulting in 6 × 2 samples. The best 2 monoliths of each series of 6 were chosen for the tests. The coated monoliths were chosen evaluating the wt% increase and the quality of the coating (homogeneity and thickness, possible partial clogging of some channels). The absolute weight and the wt% increase of each prepared monolith are reported in Table 1. Monoliths 2, 4, 7 and 11 were used in the activity tests. All the monoliths gained a very similar weight, confirming that the slurry was homogeneous and that the procedure is reproducible. Monoliths 2 and 7 were further reduced in 20 vol.% H_2 in N_2 at 400 °C for 30 min, prior to testing.

Each monolith has 400 cells/in.^{2} (CPI), 10 mm length, square channels with 1.1 mm internal size and a wall thickness of 0.2 mm, after washcoating. Fig. 1 shows a cross section of the monolith used in the tested. Each monolith was obtained from larger samples and has an approximate round cross section to fit a tubular reactor. The circle surrounding the monolith in Fig. 1 represents a cross section of the quartz tube used as reactor during the activity tests. The coated monolith was wrapped in a quartz wool tape in order to seal it in the tube and avoid bypass of gas in between the monolith and

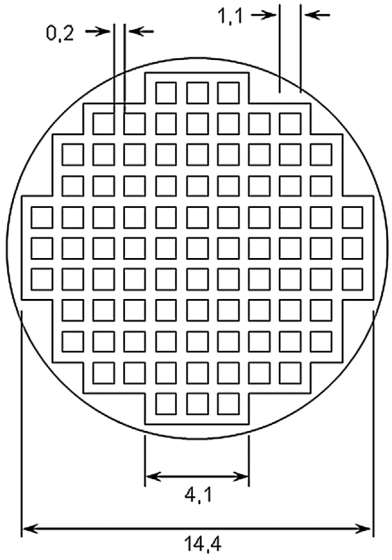

Fig. 1. Cross section of the monolith used in this work. Sizes are in mm, after the washcoat.

Table 1
Measured weight of the blank and coated monoliths, for each catalyst prepared.

Rh/ZrO_2						
Monolith n°	1	2	3	4	5	6
Initial weight (g)	0.729	0.740	0.756	0.778	0.736	0.746
Weight after coating	0.851	0.865	0.883	0.911	0.872	0.871
Coating wt%	14.3	14.5	14.4	14.6	15.6	14.4
$Rh/CeO_2–ZrO_2$						
Monolith n°	7	8	9	10	11	12
Initial weight (g)	0.753	0.710	0.747	0.719	0.710	0.784
Weight after coating	0.887	0.833	0.872	0.843	0.836	0.925
Coating wt%	15.1	14.8	14.3	14.7	15.1	15.2

the tube. In the following, the Rh/ZrO_2 and $Rh/CeO_2–ZrO_2$ samples will be referred to as Z and CZ, respectively.

2.2. Catalyst characterization

The surface area and the porosity were measured with a Micromeritics ASAP 2000 unit. The samples were de-gassed by evacuation at 250 °C for a minimum of 4–5 h prior to analysis. Data were collected at liquid nitrogen boiling temperature (77 K). The surface area was calculated by the BET (Brunauer–Emmett–Teller) method with data collected at relative pressures between 0.06 and 0.2. The total pore volume was measured at p/p_0 of 0.99. The pore diameter distribution was determined using the BJH (Barrett–Joyner–Halenda) method.

X-ray diffraction patterns (XRD) were obtained using a Siemens D5000 diffractometer with a Cu Kα monochromatic radiation, a scanning range 2θ between 10 and 90°, a step size of 0.02° and a time/step ratio of 1.0 s.

Temperature programmed reduction (TPR) and oxidation (TPO) tests were performed with a Micromeritics Autochem 2910 equipped with a TCD detector. The samples were flushed in helium at 250 °C for 2 h prior to analysis and cooled down to room temperature. The analyses was carried out using 5% H_2 in Ar or 5% O_2 in He, with a heating rate of 10 °C/min, up to 850 °C.

The metal dispersion and the average particle size were estimated by means of H_2 chemisorption, using a Micromeritics ASAP 2020 unit. The samples were evacuated in helium at 40 °C for 60 min, then reduced in H_2 at 650 °C for 60 min. The reduction was followed by evacuation in H_2 at 400 °C, for 240 min. The analysis was performed dosing H_2 at 40 °C, assuming a H:Rh stoichiometric ratio of 1:1. According to Gatica et al. [38], a suitable temperature for measuring Rh dispersion on ceria–zirconia supports is −80 °C. However, several authors carry out H_2 chemisorption on similar systems at $T > 30$ °C [39–42]. Our apparatus cannot run analysis below room temperature, so it was not possible to determine the chemisorption at the conditions used in [38]. Still, we believe that our data are meaningful, since the focus is on the change of the dispersion of the different samples, as discussed in the following paragraphs. Therefore, the differential values are more important than the absolute precision of the measurements.

2.3. Activity tests

Activity tests were carried out in a continuous flow reactor operating at nearly atmospheric pressure. It consist of a quartz tube, 16 mm inner diameter, placed inside an electrically heated furnace to reach a uniform temperature along the tube. The catalyst monolith is at the center of the tube; further details can be found in [43]. The furnace is operated by a programmable controller. The temperature was ramped up and down at a constant rate. Thermocouples (K-type) were also inserted at the inlet and outlet of the catalyst. Three different inlet gas mixtures were used, with 3.33% CH_4 and variable O_2, from 1.67% to 2.33%, using nitrogen as an inert. Diluted conditions are necessary to better control the catalyst temperature, being exo- and endothermic reactions involved. Table 2 summarizes the composition of the feed tested to study the fuel/air ratio, together with the equivalence ratio, ϕ, defined as the actual fuel to air ratio divided by the stoichiometric ratio of the total oxidation reaction, and with the lambda value, $\Lambda = 1/\phi$. Partial oxidation implies fuel-rich ($\phi > 1$) mixtures, and the precise CPO stoichiometric ratio is equal to $\phi = 4$ (i.e., 1/4 the O_2 required for total oxidation). The standard conditions during the activity test were total gas flow (at 20 °C) 2570 ml/min, resulting in a quite high GHSV = 100 000 h^{-1}. The temperature was cycled between 300 °C and 850 °C, to scan different reacting temperatures, with a heating rate of 10 °C/min and free cooling.

Reactants and products were analyzed by paramagnetic (O_2), thermal conductivity (H_2) and IR spectroscopy (CH_4, CO, CO_2) techniques.

Water was removed from the exhaust gas by condensation prior to analysis. Results are reported in terms of molar fractions, conversion and selectivity. Conversion, a concise indication of the reaction progress, is defined through the CH_4 molar flow rates, N_{CH_4}, in and out:

$$\Gamma_{CH_4} = \frac{N^{in}_{CH_4} - N^{out}_{CH_4}}{N^{in}_{CH_4}} \times 100 \quad (1)$$

The conversion is not fully informative of the reaction course, since the carbon and hydrogen atoms from the reacted CH_4 might either combine into total oxidation species (CO_2 and H_2O) or partial oxidation species, namely syngas (CO and H_2). Selectivity to one product with respect to all the others is required. We used the hydrogen selectivity, defined as the ratio:

$$S_{H_2} = \frac{H_2}{H_2 + H_2O} \quad (2)$$

based on either concentrations or mole fractions. The complement to unity of hydrogen selectivity is water selectivity. Similarly, we defined CO selectivity as:

$$S_{CO} = \frac{CO}{CO + CO_2} \quad (3)$$

and its complement to unity is CO_2 selectivity.

Results were also compared with the equilibrium composition, calculated by mixture Gibbs free-energy minimization, under isenthalpic and isobaric conditions to simulate the adiabatic reactor.

Table 2
Volumetric composition of the gas mixtures fed with corresponding equivalence ratio and the lambda value.

Mixture	CH_4 [vol.%]	O_2 [vol.%]	N_2 [vol.%]	φ	Λ
Mix1	3.33	1.67	95.00	4.00	0.25
Mix2	3.33	2.00	94.67	3.33	0.30
Mix3	3.33	2.33	94.34	2.86	0.35

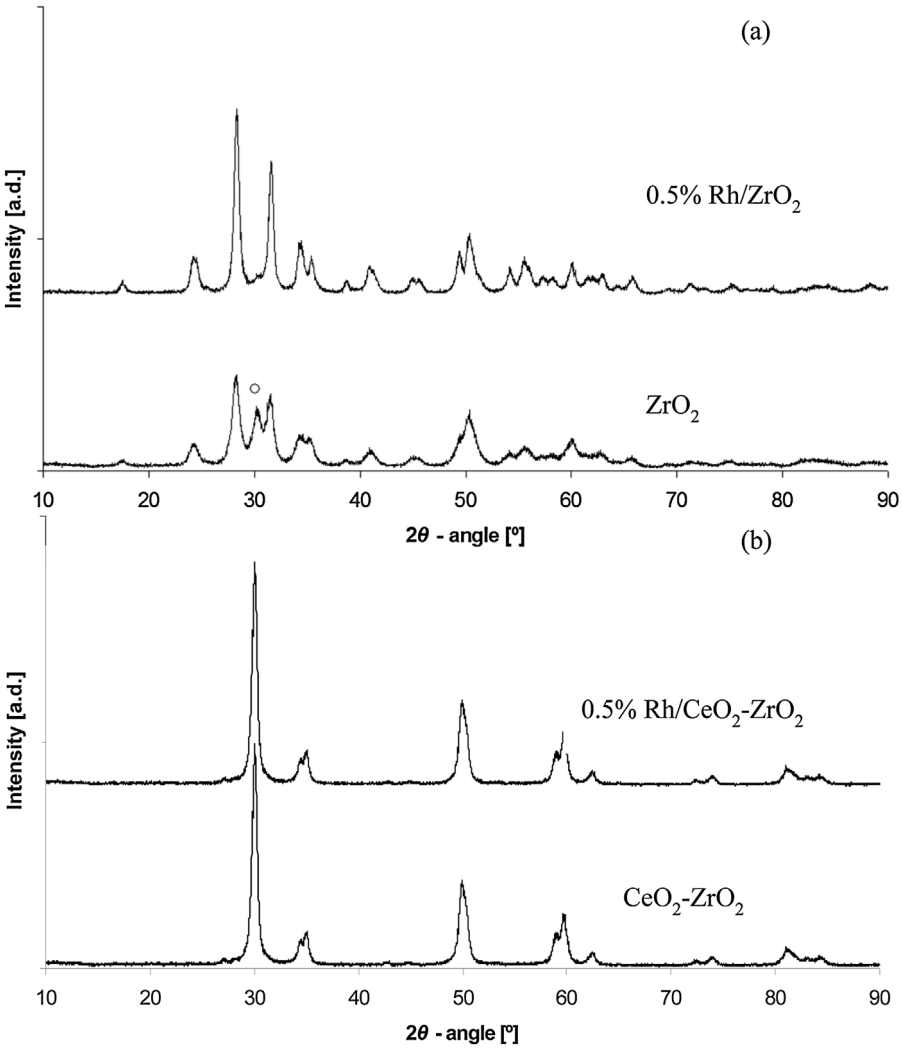

Fig. 2. XRD patterns of catalyst powders based on zirconia (a) and ceria–zirconia (b), comparison before and after impregnation with Rh and second calcination.

Since the minimization under mass conservation constrains is not trivial, we used the Cantera [44] implementation, based on VCS algorithm and the NASA thermodynamic database.

3. Results and discussion

3.1. XRD

The XRD patterns for both catalysts are shown in Fig. 2 and compared with the bare supports. The morphology of zirconia changed when calcined at 800 °C; the tetragonal phase of ZrO_2 (the peak at 30.1°, marked in Fig. 2a), turned into monoclinic phase (peaks at 28.4 and 31.6) after calcination in air at 800 °C for 4 h.

Ceria-doped zirconia did not change the morphologic configuration (Fig. 2b); all the peaks show the formation of a solid solution of $Ce_{0.16}Zr_{0.84}O_2$, which is the tetragonal phase of ZrO_2. Indeed, both the blank and the impregnated sample show a peak at 30, overlapping with one given by zirconia at 30.1°. Furthermore, a pair of peaks is detected at 34.6 and 35.1°, and they are very close to those given by tetragonal zirconia at 34.5 and 35.3°. The small shift is due to the presence of cerium in the lattice. Similar interpretation were previously reported by Hori et al. [45] for $Ce_{0.25}Zr_{0.75}O_2$ and Passos et al. [46] for $Ce_{0.16}Zr_{0.84}O_2$. Both for the Z and CZ samples, no rhodium phases were detected because of the small concentration of rhodium in the powder.

3.2. Porosity analysis

The results of the porosity analysis are summarized in Table 3, together with the catalysts and supports main features. The total surface area of the original ZrO_2 support is much higher than in the CeO_2–ZrO_2 support, but after calcination the 0.5% Rh/CeO_2–ZrO_2 showed only a slight decrease, while the 0.5% Rh/ZrO_2 lost half of its surface area, which is now slightly lower than the CeO_2–ZrO_2 based catalyst, even if comparable.

It is noticeable how the drop in surface area value is much larger for the Z sample compared to the CZ one. The reason for the different drop is likely due to the simultaneous presence of ceria and zirconia in the support and the formation of a thermally stable solid solution. Indeed, it is well known that mixed oxide supports of this kind exhibits a higher thermal stability compared to the pure compounds. Several examples can be found in [47,48].

The data reported in Table 3 are very accurate, being the calculated standard deviation very small. Furthermore, the correlation coefficients of the curves interpolating the adsorption isotherms range within 0.999990 and 0.999999, confirming both the high precision and accuracy of the analysis results.

3.3. Chemisorption

As summarized in Table 4, the dispersions detected right after calcining the samples at 800 °C were not very high; being 6.6 and

Table 3
Structural characterization of the rhodium catalysts. The relative standard deviation on the reported numbers is always <0.2%.

	ZrO_2	0.5% Rh/ZrO_2	CeO_2–ZrO_2	0.5% Rh/CeO_2–ZrO_2
BET surface area [m^2/g]	87	43	57	49
Total pore volume [cm^3/g]	0.221	0.146	0.175	0.173
Average pore diameter [Å]	102	135	123	142
Observed phases	Tetrag. and monocl. ZrO_2	Monocl. ZrO_2	Tetrag. ZrO_2	Tetrag. ZrO_2
Calcination	500 °C, 5 h in air	800 °C, 4 h in air	500 °C, 5 h in air	800 °C, 4 h in air

15.2% for the Z and the CZ supported samples, respectively. Accordingly, the particles are bigger for the zirconia sample than for the one supported on the mixed oxide. Interestingly, the dispersion of the CZ sample considerably increased after a sequence of repeated TPR's and TPO's. Indeed, after the redox treatment, the dispersion is found to be 33% higher than in the freshly calcined sample, meaning that the redox treatment caused a modification of the catalyst surface, resulting in smaller, better dispersed particles. For the Z sample, a more limited increase of the dispersion was detected after the same sequence of TPR/TPO. As discussed in the introduction [26–29], the observation agrees with the reported properties of ceria, which is often used both as support stabilizer and dispersion promoter. The obtained TPR peaks, as discussed further on, also confirm these results. In the literature, several examples can be found of $Ce_xZr_{1-x}O_2$ mixtures increasing the dispersion of different metals, such as Pt [46,49], Pd [15,16], Rh [27,50], Ni [17,18]. As for the porosimetry analyses, also for the chemisorption measurements the relative standard deviations are small and the correlation coefficients of the interpolating curves close to 1, meaning that the reported numbers are accurate and statistically different.

3.4. Conditioning

In our experience, catalysts being tested, often need some preliminary heating/cooling cycles under reaction feed, to achieve stable performance. For this reasons the prepared samples are always exposed to the reaction mixture while the temperature is quickly ramped up and down, at the beginning of every test-campaign. We call the preliminary cycles catalyst "conditioning". The activity of the samples used in this work was indeed observed to vary in time since their first use; it increased after some heating/cooling cycles up to a stable value, notwithstanding the previous double calcination (of the catalyst and of the monolith). Therefore, each sample was conditioned and the conditioning period was studied using Mix1 ($\Lambda = 0.25$), by monitoring CH_4 conversion during subsequent cycles. Results for both type of catalysts are reported in Fig. 3.

For the Z catalyst, Fig. 3a, 11 fast (20 °C/min) heating cycles were followed by a slower one (10 °C/min). All tests were run in a sequence, taking several days. Results for 5 of the 12 ramps are reported, for easier readability, namely ramps 1, 2, 4, 10 and 12. Except for the first cycle, in all the curves the ignition temperature is always the same. However, the activity at higher temperature increases gradually between cycles, stabilizing after the 10th cycle.

The conversion of CH_4 at the highest temperature, increased by about 20% between the 2nd and the 10th ramp. Accordingly, quite a long conditioning is required to achieve stable performances of the Z catalyst.

With the CZ sample, only four ramps were required, three fast and one slow, Fig. 3b. Quite interestingly, the conditioning of the CZ catalyst shows a much faster approach to the steady state. Already at the second cycle, the catalyst shows nearly stable performances, both at the ignition and at higher temperature. The presence of Ce allows achieving a higher conversion at high temperature, as apparent from Fig. 3, and also lowers the ignition temperature of about 60 °C. The main products detected during the conditioning ramps of Rh/ZrO_2 are CO_2 and H_2O (calculated) up to 750 °C, when H_2 and CO start forming and quickly increase their concentration, while the total oxidation products slowly decrease (see also Fig. 7, discussed later). On repeated heating cycles, the total oxidation products keep a constant concentration around the ignition temperature, but they progressively decrease in favor of partial oxidation species above 550–600 °C. In other words, cycle after cycle, the selectivity toward H_2 and CO increases until stabilization at the end of the conditioning procedure. The implications of the detected product composition will be discussed later. So far, remind that after the ignition, partial oxidation products are formed and the atmosphere along the catalyst bed changes from oxidizing, because of the presence of O_2, to reducing, due to the lack of oxygen and the formation of increasing amounts of H_2 and CO. The conditioning procedure clearly points out that the catalyst properties are changing due to either progressive reduction and re-oxidation or to a re-construction of its surface. Similar behaviors have previously been reported by Eriksson et al. [28] for 1% Rh on the same supports and also by Bruno et al. [35] for 0.5% Rh supported both on alumina and on zirconia. Although the authors did not provide a specific explanation for the phenomena detected, they both concluded that the conditioning process is not simply due to a progressive reduction of the catalyst, since pre-reduced samples exhibited the same behavior. Beretta et al. also investigated the conditioning of catalyst for partial oxidation of methane in two separate works [33,34], both with Rh on alumina. In the first one, the existence of a conditioning period is highlighted and explained with a reconstruction of the Rh particles, through a progressive loss of defects sites. In the second contribution, the authors investigate the effect of three different preparation procedures and conclude that the conditioning of the catalysts is explained by a restructuring of the Rh particles through the reorganization of isolated atoms and the aggregation of small particles into bigger ones.

Table 4
Dispersion and particle size determined by H_2 chemisorption for the fresh samples and after the sequence of TPR's and TPO's. The relative standard deviation ranges between 1.04 and 3.23 %.

Sample	Dispersion (%)	Average particle size (nm)
Rh/ZrO_2 fresh	6.6	16.6
Rh/ZrO_2 TPx	7.9	13.9
Rh/$Ce_{0.16}Zr_{0.84}O_2$ fresh	15.2	7.2
Rh/$Ce_{0.16}Zr_{0.84}O_2$ TPx	20.2	5.5

3.4.1. Catalyst aging

During the last conditioning cycle, the catalyst achieved stable and reproducible activity. The stability was further investigated at high temperature for a longer time.

The tests shown in Fig. 4, were run with the standard gas composition at $\Lambda = 0.25$. A heating cycle up to 850 °C was set, followed by cooling down to 250 °C in order to verify that the catalyst was performing as in the last of the conditioning ramps. The temperature was then increased again to the value set for the aging test and held for 6 h. During the step at constant temperature, all the

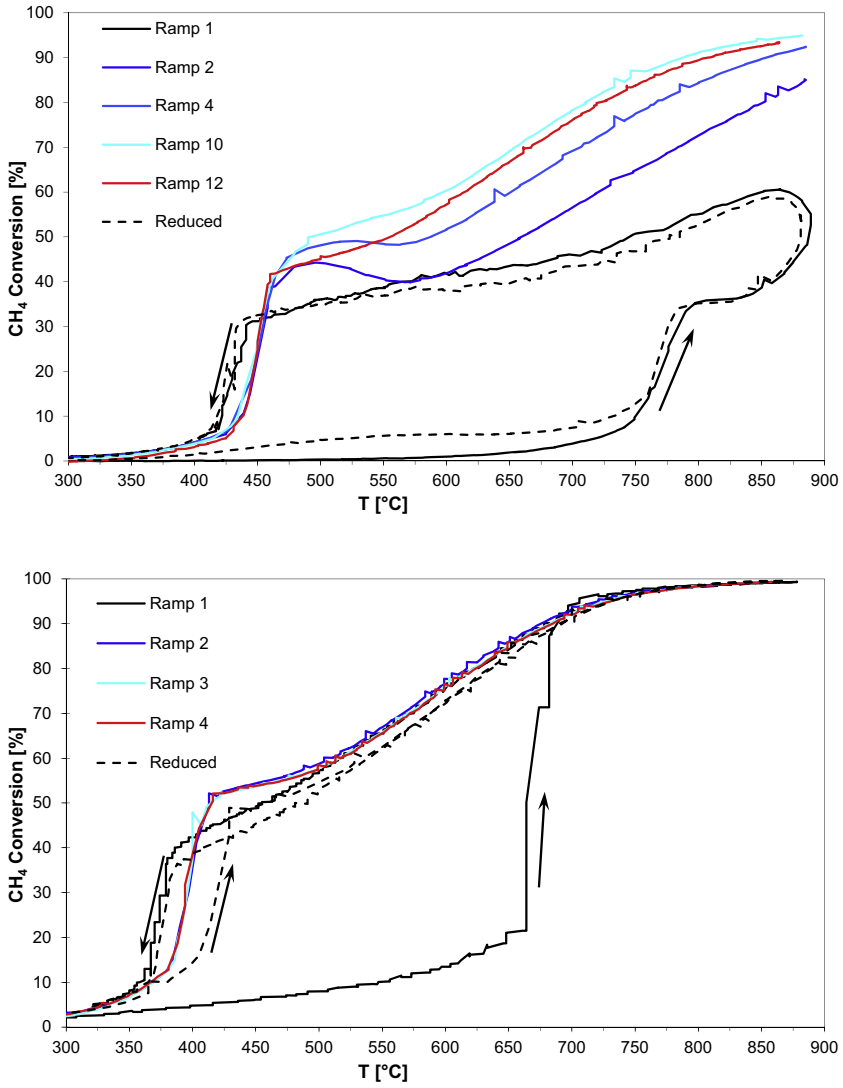

Fig. 3. CH_4 conversion vs. catalyst inlet temperature during conditioning. Mix1 in the feed, under standard conditions. (above) Rh/ZrO_2, (below) Rh/CeO_2–ZrO_2. The arrows show whether the temperature is increasing or decreasing.

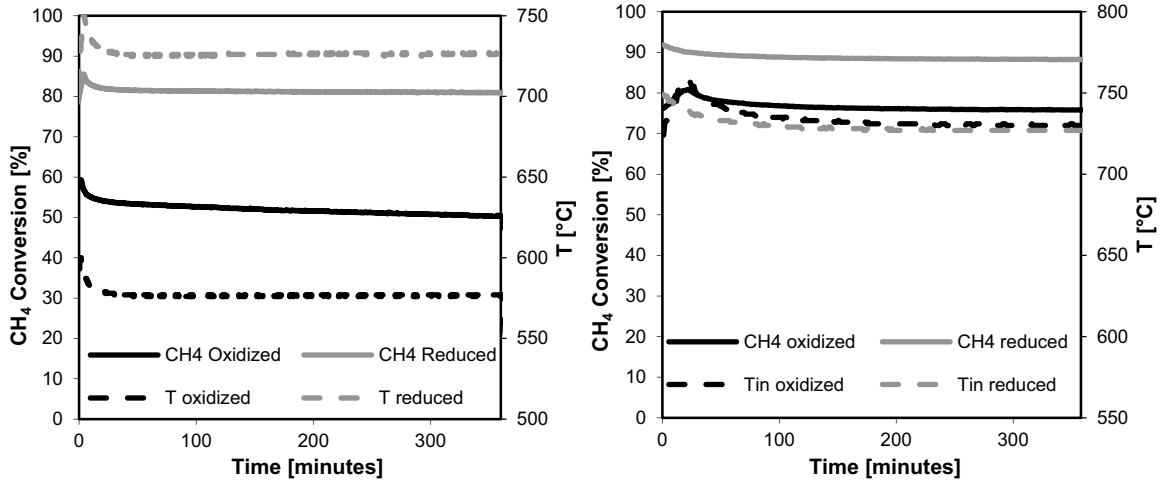

Fig. 4. Methane conversion and catalyst inlet temperature as a function of the time on stream for Rh supported on zirconia (left panel) and on ceria–zirconia (right panel).

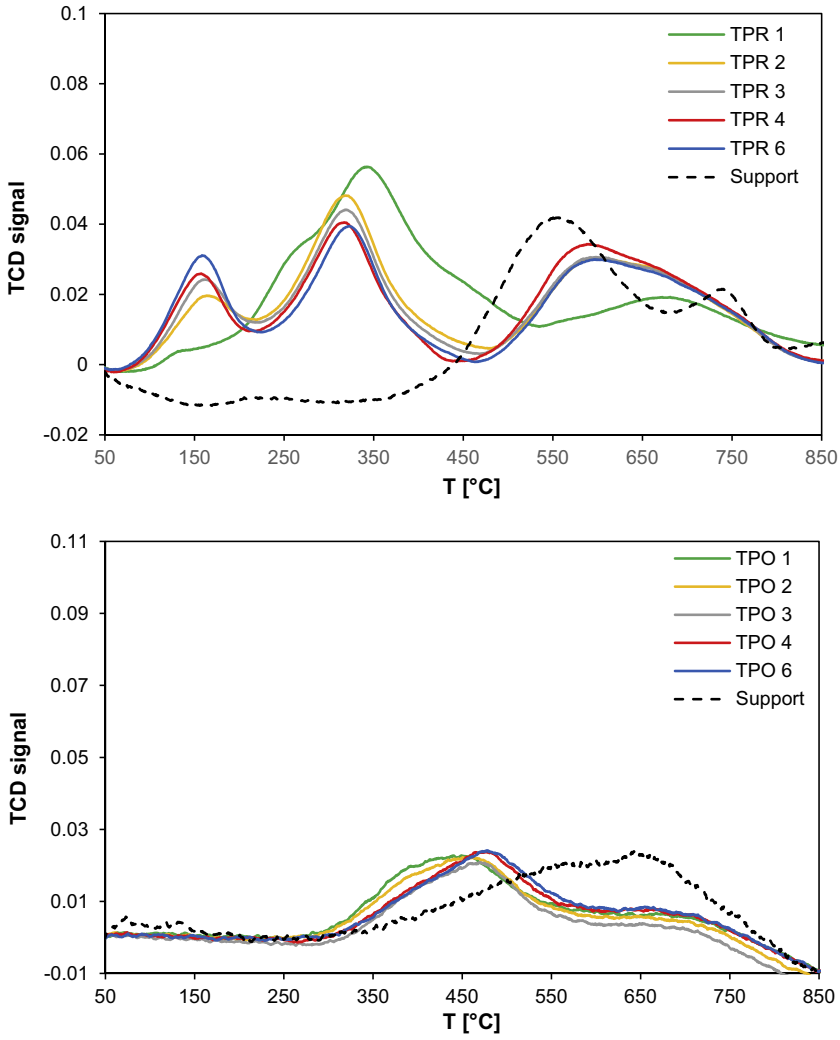

Fig. 5. Repeated TPR (above) and TPO (below) profiles on Rh/ZrO_2. Each TPR was followed by a TPO.

samples exhibited a high stability, with the methane conversion holding a constant value. Only the Z sample calcined in air showed a slight decrease of the conversion. Deactivation is not the focus of this work, which instead deals with the phenomena occurring during the conditioning process. However, the conditioning period and the runs reported in Fig. 4, add up to 30 h for the Z sample and to about 20 h for the CZ sample: at the end of this period the catalysts exhibit and overall stable behavior.

At the end of each series of tests, weighting proved the absence of any loss of active material and the monolith appeared still homogeneously coated, meaning that the powder was adhering well to the ceramic substrate and the washcoating was done properly.

Table 5
Measured H_2 uptake for each repeated TPR. Only the consumption calculated from the peaks matched with the Rh reduction is quantified.

TPR n	μmol H_2/g_{cat}	
	Rh/ZrO_2	$Rh/Ce_{0.16}Zr_{0.84}O_2$
1	184	453
2	129	459
3	120	436
4	108	661
6	112	704

3.5. TPR and TPO

A sequence of repeated TPR's and TPO's was performed on both the zirconia and ceria–zirconia supported samples. Each cycle include a TPR followed by a TPO. These measurements are designed to clarify what happens on the catalyst surface during the conditioning procedure. Exposing the catalyst to an atmosphere that repeatedly switches between reducing and oxidizing, allows simulating the atmosphere of the activity tests. Indeed, during the partial oxidation tests, when the fed methane and oxygen are consumed to form H_2 and CO, the atmosphere changes from oxidizing to reducing and vice versa when the temperature is lowered and the reaction extinguishes. The results are shown in Figs. 5 and 6. They appear very interesting, reporting an evolution of the peaks assigned to the reduction of Rh species. According to the literature, the reduction of zirconia occurs at temperatures around 650 °C [17], but the peak can be very broad and extend between 500 and 850 °C. The wide reduction peak is due to the reduction of Zr^{4+} to Zr^{3+} occurring only on the surface and some of the sub layers [51]. Pure ceria gives 2 separate reduction peaks, one at around 500–600 °C, due to the reduction of surface layers and another one at around 800–950 °C, corresponding to the reduction of ceria in the bulk phase [17,52,53]. When mixed $Ce_xZr_{1-x}O_2$ oxides are formed, the reductions peaks of pure ceria and zirconia phases merge into one single, wide peak that shifts position depending on the value of

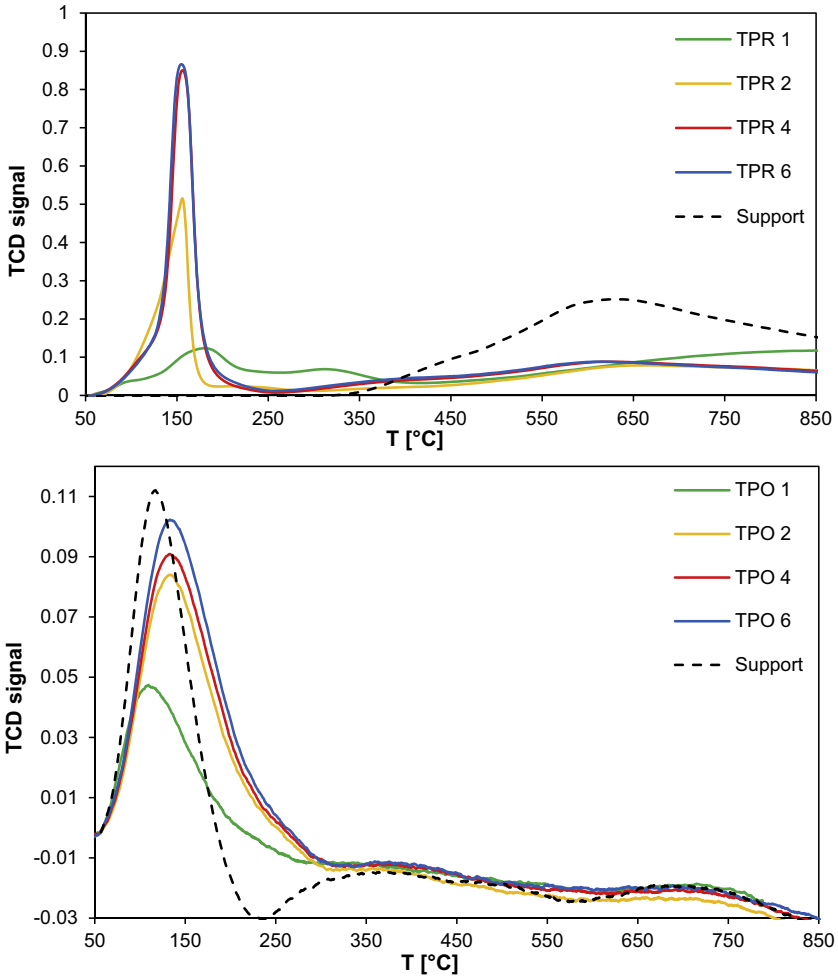

Fig. 6. Repeated TPR (above) and TPO (below) profiles on $Rh/CeO_2–ZrO_2$. Each TPR was followed by a TPO.

x, between 400 and 650 °C [17,53–55]. This is consistent with the formation of a single homogeneous solid solution.

3.5.1. Rh/ZrO_2

Fig. 5 shows the results for the zirconia supported sample. The consumption of H_2 is very low (see Table 5, column 1), meaning that both the metal and the support are hardly reducible. Three different peaks are detected at around 160, 320 and 600 °C. During the first run, the peaks overlap, while in the following TPR's they become and remain separate. The wide peak between 500 and 800 °C is due to the reduction of ZrO_2, as discussed above. The other two peaks at lower temperature are due to the reduction of surface and bulk Rh_2O_3 [27,56]. The peaks are detected at higher temperature compared to the mixed oxide sample (Fig. 6, commented below) since the Rh/ZrO_2 system without ceria is far less reducible.

This is also confirmed by the amount of H_2 consumed, reported in Table 5, which is 4–6 times lower than that of Rh supported on ceria–zirconia. The presence of Rh seems to modify the behavior of the support. Indeed, the bare zirconia powder shows two overlapping peaks at 550 and 750 °C, which are assigned to the reduction of surface and bulk ZrO_2, respectively. The TPR's of the impregnated powder show, instead, a single wide peak between 500 and 800 °C, which is possibly the combination of the two separate peaks detected on the support. All the repeated TPO measurements on Rh/ZrO_2 behave similarly, exhibiting partly overlapping peaks in the temperature range between 300 and 800 °C. These peaks match rather well with the results reported by Jóźwiak [57]. Accordingly, the peak between 300 and 550 °C is assigned to the oxidation of surface Rh and to a partial oxidation of the support, while the peak at higher temperature is the combination of the overlap of the oxidation of bulk Rh and the complete oxidation of the support. The TPR and TPO trends for the ZrO_2 supported sample are in line with its low dispersion and big particle size measured by chemisorption. All the repeated TPO measurements on Rh/ZrO_2 behave similarly, showing partly overlapping peaks in the temperature range between 300 and 800 °C.

3.5.2. $Rh/CeO_2–ZrO_2$

Regarding the CZ sample (Fig. 6), in the first TPR, three small and broad peaks of H_2 consumption are detected below 400 °C, at approx. 90, 180 and 315 °C. A forth, very wide peak in the curve is also detected above 500 °C.

The peaks below 200 °C are due to the reduction of Rh_2O_3. TPR 2–6 all show a wide peak between 450 and 750 °C, corresponding to the reduction of the mixed ceria–zirconia oxide, while TPR 1 shows a much wider peak that continues above the highest temperature investigated; in this case the reduction of deep bulk phase is likely occurring. Regarding Rh, the trend is more complex, with the peaks shifting and changing size. The sequences TPR–TPO imply that Rh was always re-oxidized before the following TPR. All the peaks detected below 200 °C correspond to the reduction of Rh_2O_3 [27,58,59]. Interestingly, the main reduction peak shifts between a TPR and the following one and it also changes its size, before stabilizing on one big, narrow peak with a maximum at 155 °C (TPR 4

and 6). An interesting work from Vis et al. [60] shows very clearly that the reduction of Rh_2O_3 can originate two separate peaks below 200 °C. The peak at lower temperature corresponds to the reduction of small, well dispersed particles, while the peak at higher temperature is due to the reduction of bulk-like, crystalline Rh_2O_3, formed by oxidation at high temperature. Accordingly, the peak at 180 °C detected in TPR1, is assigned to the reduction of bulk Rh_2O_3, while the other lower temperature peaks detected in TPR 2–6 are assigned to smaller, better dispersed Rh_2O_3 particles. The clear shift of the reduction peaks in the repeated TPR suggests that the catalyst goes through a progressive, rather slow evolution of its structure forming metal particles of different, progressively smaller size, until a final stable configuration is reached, as shown from the overlapping peaks of the last TPR's. Other authors detected the same behavior for Rh supported on $Ce_xZr_{1-x}O_2$ mixed oxides [56,58,61].

The evolution of the TPR peaks also suggests that the metal dispersion is increasing, since the H_2 consumption progressively increases, too (Table 5), meaning that more rhodium is reduced. This is also confirmed by the increase in the size of the oxidation peaks detected in the TPO's. Even though the O_2 consumption was not measured, the analyses were run in a sequence, on the same sample (i.e., on the same amount of powder); therefore, an increasing size of the oxidation peaks, reveals that more Rh is oxidized step by step. The same effect on the TPR peaks would be obtained by a decrease of the particles size, provided that all the metal remains on the surface and does not get embedded into the support. As a matter of fact, dispersion and particle size are related and inversely proportional. The TPO's show a main peak between 50 and 170 °C for the bare support together with two small peaks between 330 and 460 and 650 and 800 °C, corresponding to the oxidation of the support. The impregnated powder exhibit the same 2 small peaks at higher temperature and a similar larger peak starting at 50 °C. In this case, though, the peak extends to about 270 °C, meaning that Rh is being reduced together with the support.

Regarding the reducibility of the bare supports, it can be noted from the TPRs that the addition of ceria to zirconia enhances it. Indeed, the reduction peak of the mixed oxide powder is considerably larger than that of the pure ZrO_2.

3.5.3. Comparison with conditioning results

Overall, the results of the TPR and TPO analyses on both the samples are consistent with the different conditioning time required by the samples. In the case of Rh supported on the mixed oxide, the TPR investigation likely reproduced the conditions and the catalyst modifications occurring during the conditioning period, highlighting a decrease of the particle average size and a consequent increase of the dispersion. This in turn favors a higher activity of the catalyst after some temperature cycles. In the case of the zirconia supported sample, the sequence of 6 TPR's and 6 TPO's was not enough to produce a significant change on the catalyst structure. However, these analyses confirm that this sample requires a much longer conditioning period to achieve a high and stable activity. It should be considered that the WHSV of the reducing gases during the CPO tests is about 3 orders of magnitude higher than that achieved during the TPR. Indeed, during the CPO tests, about 0.15 g of catalyst were exposed to up to 150 ml/min of formed H_2 (at the highest temperature and yield reached): a much greater amount compared to the TPR experiments, where about 0.4 g of catalyst were exposed to 10 ml/min of 5% H_2 in Ar. Furthermore, other reducing gases such as CH_4 and CO were also present in the CPO gas mixture that contributed to the progressive reduction of the metal. The same considerations apply to the amount of O_2/oxidation species used during the TPO and the CPO experiments. Considering the large difference in the ratio between the reducing/oxidizing agents and the catalyst amount during the TPx experiments and the CPO runs, it is surprising that such considerable changes in the structure of the $Rh/CeO_2–ZrO_2$ sample were detected during TPx tests. Consistently, the changes on the surface of the catalysts occurring during the conditioning period are likely to be similar but larger than those highlighted with the different analyses. Unfortunately, running TPR/TPO and chemisorption on the tested samples was not possible due to the low amount of powder that can be recovered from the coated monoliths after the tests, which would also be possibly contaminated by variable amounts of cordierite from the monoliths.

As anticipated in Section 3.4, other authors reported conditioning periods for similar catalytic systems and gave different interpretations. In our case, the increase in activity appears to be the effect of a restructuring of the surface, resulting in an improved dispersion of the active phase (i.e., a higher number of available Rh active sites), caused by repeated reduction and oxidation steps. Also, our results provide evidences that the progressive change of the catalyst performance is not simply due to a reduction of the metal particles. We believe that the tests on pre-reduced catalysts reported in Fig. 3 support our interpretation. Indeed, the figure also reports the methane conversion curves detected on the first run carried out with the samples pre-reduced in H_2. In the case of the Z sample, there is a very limited difference with the non-reduced one. The methane conversion is slightly higher at all the temperatures and suddenly jumps, above 750 °C. The following conditioning cycles were very similar to those of the non-reduced sample and it took again 12 cycles to reach steady performance.

For the CZ sample, instead, the reduced catalyst exhibits an activity very close to the final one achieved by the non-reduced sample. Nonetheless, important differences are still detected, such as a considerably higher ignition temperature and a lower methane conversion up to 650–700 °C. These results are in agreement with the findings in [28,35]. However, the authors there exclude that the reduction of the catalyst plays a role in the conditioning, while Fig. 3 as well as our TPR/TPO analyses suggest that the reduction is the cause of the reconstruction of the catalyst surface. If reduction was the only reason for the initial catalyst instability, a pre-reduced sample should exhibit good and stable conversion/selectivity since the first cycle. This is not the case with our catalysts.

Indeed, our results point out that during the conditioning cycles, the catalysts are reduced when the temperature increases and re-oxidized when the temperature is lowered to the starting value. These experimental evidences further confirm that the catalyst undergoes a process of reduction and re-oxidation during the temperature cycles, which causes a change of its structure. In particular, the activity test results combined with those of the repeated TPR/TPO and the dispersion measured before and after that (see Table 4), show that the Rh metal particles reduce their size with a consequent increase of the metal dispersion. The phenomenon is much faster for the sample containing ceria, which increases the reducibility of the catalyst, and therefore, facilitates a faster achievement of a higher metal dispersion. Once the conditioning is complete and the catalysts reach stable performance, the surface is still very likely undergoing repeated oxidation and reduction cycles, but without any further structure modification. Several authors clearly showed that under CPO reaction conditions, the catalyst surface switches between an oxidized and a reduced state, at least when a dry and steam reforming step follows a complete methane oxidation stage [19,62–64]. Specifically, at the lower temperature, when no reaction or just the total methane oxidation occur, syngas concentration is negligible or small; at this conditions, we expect the metallic catalyst to be in an oxidized state. Afterwards, at higher temperature, oxygen is completely consumed, reducing gas concentration grows, starting from the reactor end; a front of reduced metal is likely to develop, starting from the end of the catalyst bed and progressively extending upstream, toward the beginning of the bed. The situation is reversed when

the temperature is decreased and the reaction switches from the reforming to the combustion step again.

3.6. Activity measurements

3.6.1. Role of (inlet) temperature

Once the catalyst reached a stable behavior in heating and cooling cycles, the heating rate was decreased, to allow the achievement of steady state conditions on the catalyst at any temperature, even if continuously varied. Indeed, a lower heating rate allows to better spot the ignition temperature. We also speculate that higher heating rates compete with the thermal inertia of the flow and monolith, affecting the release of reaction heat, possibly resulting in a mismatch between measured and actual temperature of the catalyst. For that reason, a lower heating rate of 10 °C/min was always used in all the activity tests.

The effect of the inlet temperature was partially anticipated in Fig. 3, in terms of CH_4 conversion. Its effect on the exit gas composition is qualitatively similar for any inlet mixture tested. We illustrate and comment the products distribution in the intermediate case of Mix2 ($\Lambda = 0.30$) on Rh/ZrO_2. To discuss the results, we consider that the global reactions listed in Table 6 may occur along the catalyst, depending on the operating conditions (i.e., temperature, inlet composition and flow rate).

The formation of the partial oxidation products can occur via R1, in which case the reaction is said to follow the so-called direct mechanism. An alternative route is the formation of total oxidation products (R2) consuming all the available oxygen. The formed CO_2 and H_2O further react with methane via dry (R3) and steam (R5) reforming reactions at higher temperatures. In this case, the reaction occurs via the so-called indirect or combustion and reforming mechanism. Whether a catalyst leads to the formation of synthesis gas through one or the other mechanism is debated in the literature [12,65]. The situation is complicated by the fact that the total or partial oxidation products can be either primary or secondary, meaning that the detection of CO_2, for example, is not a conclusive evidence of the indirect mechanism occurring. Indeed, CO_2 and H_2O can be the result of the reaction of promptly formed, primary CO and H_2 with residual amounts of oxygen in the gas stream [66]. The situation can be even more complex with only CO being a primary product and further react to form CO_2, while H_2 is a secondary product formed via indirect oxidation [67]. In the latter case, the authors state that the classical distinction between direct and indirect mechanism is not meaningful, since CO and H_2 can be formed via different routes.

Table 6 also reports the oxidation of both carbon monoxide and hydrogen. These reactions likely have a very limited role in the global mechanism, but they can occur in a narrow time and space window when/where CO, H_2 and O_2 are present at the same time. It is the case of the region between 450 and 470 °C in Fig. 7, where O_2 is not yet completely consumed and CO and H_2 are already formed.

Fig. 7 shows the product composition varying the inlet temperature. Since H_2O was not measured, it was obtained from H and O atom balances, with a mean square errors technique (being 2 atomic balances sharing the same single unknown, i.e., the amount of H_2O). Although plots like Fig. 7 are conventional reports of activity measurements, it should be remarked that each point on a curve (i.e., results at a given pre-heating temperature) reflects the outlet of an independent steady state operation of the reactor. Each data set at given inlet temperature, comprising the mole fractions of the species CH_4, O_2, H_2O, CO_2, H_2 and CO, is only a function of the corresponding inlet temperature, (and composition and flow rate, kept constant in the results of Fig. 7), and it is not related to the neighboring experimental points at higher or lower temperature, beside the chronological order. To better explain the concept with an example, the CO_2 profile in Fig. 7, shows a maximum and then decreases with temperature: that does not necessarily mean that CO_2 at higher temperature has been consumed (e.g., by Reaction R3), but that the combination of all Reactions R1–R8, at that temperature, yields a smaller amount of CO_2 in the products, if compared with a lower inlet temperature. Possibly, CO_2 was never higher than the outlet in any point of the reactor.

For the Z sample, the lowest temperature to observe any conversion at the given residence time (GHSV = 100 000 h^{-1}, about 25 ms) is approx. 350 °C for both catalysts at any inlet composition. Methane total oxidation (R2) occurs at lower temperature, as clearly shown by the products (H_2O and CO_2, at the R2 stoichiometry). The remaining reactions start abruptly (ignition) at about 450 °C, depending on the catalyst sample; methane conversion, quite small at lower temperature, reaches about 50% at about 450 °C. The value of methane conversion after ignition means that the methane not only reacted according to the total oxidation reaction (which would have led to a 25% conversion), but some partial oxidation (R1) products are formed, as well. As a matter of fact H_2 and CO appear among the products only above 450 °C. After

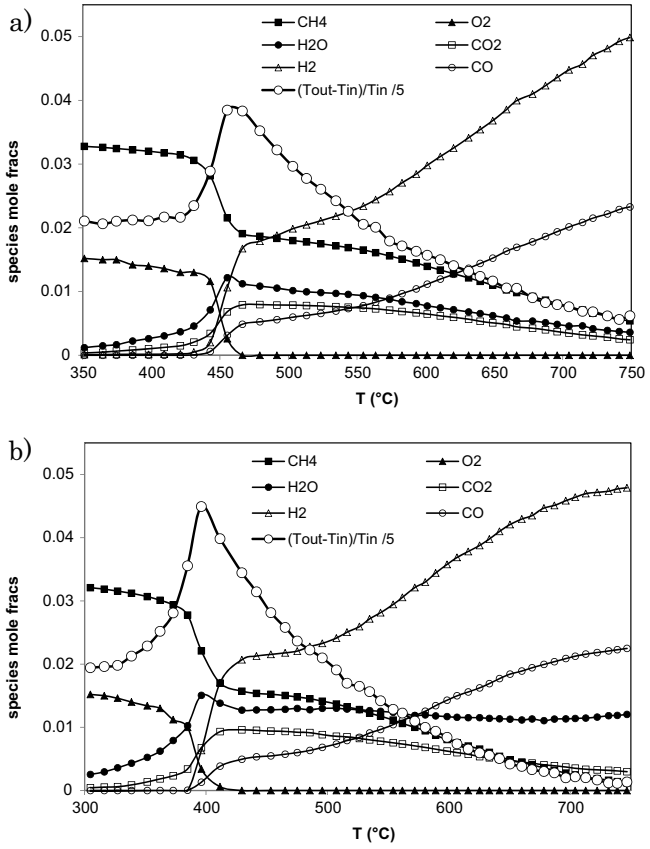

Fig. 7. Composition measured in the outlet, varying the inlet temperature. Rh/ZrO_2 catalyst (a) and Rh/CeO_2–ZrO_2 (b). $\Lambda = 0.25$. H_2O is calculated.

Table 6
Global reactions occurring in CPO.

#	Reaction	ΔH_R [kJ/mol]	
R1	$CH_4 + 1/2\,O_2 \Leftrightarrow CO + 2H_2$	−36	methane partial oxidation
R2	$CH_4 + 2\,O_2 \Leftrightarrow CO_2 + 2H_2O$	−803	methane total oxidation
R3	$CH_4 + CO_2 \Leftrightarrow 2H_2 + 2CO$	247	methane dry reforming
R4	$CO + H_2O \Leftrightarrow CO_2 + H_2$	−41	water-gas shift
R5	$CH_4 + H_2O \Leftrightarrow 3H_2 + CO$	206	methane steam reforming
R6	$C + O_2 \Leftrightarrow CO_2$	−393	carbon oxidation/deposition
R7	$CO + 1/2\,O_2 \Leftrightarrow CO_2$	−283	Carbon monoxide oxidation
R8	$H_2 + 1/2\,O_2 \Leftrightarrow 2H_2O$	−286	Hydrogen oxidation

the ignition temperature, the residual O_2 in the products is zero, which leads to a convenient definition of ignition temperature as the 50% conversion O_2. After all the oxygen is consumed, a further methane conversion is difficult to achieve, requiring significantly higher temperature to increase appreciably. H_2O and CO_2 decrease in the products after the maximum at the ignition T, while H_2 and CO increase monotonously as the temperature rises.

Fig. **7** also shows the variation of the outlet temperature with respect to the inlet value during the test, $(T_{out}-T_{in})/T_{in}$, divided by 5 to fit it to the Y axis. The traced curve highlights that, notwithstanding the diluted conditions, the heat of reaction affect the temperature of the gases at the outlet of the monoliths. It is very interesting to note that the curve peaks in correspondence of the maximum amounts of CO_2 and H_2O, while it approaches zero (meaning no difference between inlet and outlet) as CO and H_2 are formed and reach their highest concentrations. Being evident from the products the development of endothermic reactions at high temperature, an outlet temperature comparable to the inlet one implies that the endothermic reactions follow exothermic ones along the monolith length, mutually compensating the reactions' heat.

For the CZ sample, similar information as those contained in Fig. 7a, can be deduced from Fig. 7b. Indeed, both CO and H_2 formation start at the same time above 450 °C. CO_2 and H_2O are, instead, formed already starting from 300 to 350 °C and reach a maximum at around 470 °C. Above this temperature, CO_2 continuously decreases, while water decreases at first and then starts increasing again above 600 °C. The effect is more pronounced for higher Λ values (see Fig. 9), as more oxygen is available. This may be an indication of the reverse water gas shift reaction (RWGS) occurring at temperatures above 600 °C, which seems to be confirmed by the high temperature trends of H_2 and CO, which tend to flatten at high temperature. Reactions (R9) and (R10) can also contribute, as discussed in Section 3.6.2. Overall, the sequence of formation of the products suggests that the catalyst is following the indirect mechanism, by combusting part of the methane with all the oxygen available and with the formed CO_2 and H_2O further reacting with the residual methane as the temperature increases.

From the composition pattern description, the presence of different chemical regimes becomes clearly visible. Below the ignition temperature, only total methane oxidation occurs, causing the outlet temperature to increase at a faster HR than the one set. At the ignition (ca. 400–450 °C in the case of Fig. 7) partial oxidation is activated, completing the oxygen consumption. The short temperature range in which that occurs is due to the local (at the catalyst surface) acceleration of reaction rates given by the release of the heat of the total oxidation reaction, resulting in an autocatalytic process. Even if CH_4 might react with other species (R3 and R5), its consumption remains limited at this temperature because those reactions clearly activate at higher temperature, on these catalysts and for the given inlet composition. A third mechanism is triggered at higher temperature, where CH_4 starts reacting with water (R5) and possibly with CO_2 (R3). Both steam (R5) and dry (R3) reforming reactions are endothermic, thus, they are strongly dependent on temperature, requiring higher temperature to yield higher methane conversion. In principle, combustion reactions can also be affected by the temperature and being exothermic their conversion should decrease as the temperature increases. In practice, they show extremely high equilibrium constants, so that the shift of conversion cannot be appreciated. Combustion keep consuming all the available oxygen (which become a limiting reactant), and the temperature does not affect significantly the equilibrium composition. In other words, partial equilibrium can be assumed for oxidations. The equilibrium constants for the reforming reactions is much smaller, so they are more affected by the temperature, compared to the combustions. The type and the concentration of the species detected suggest that the catalyst is following the indirect mechanism, with a first initial total oxidation step followed by a second steam and dry reforming one. An overall negligible production/sink of heat means, that the endothermic reforming reactions are compensated by some exothermic ones. Once again, that supports the model of oxidation occurring in the first part of the catalyst bed and endothermic reforming in the latter.

3.6.2. Effect of catalyst support and inlet composition

The performance of the two Rh catalysts, based on two different supports, was compared under different O_2/fuel ratios, gradually increasing above the CPO stoichiometry (see Table 2). All tests used a heating rate of 10 °C/min and data collected after catalyst conditioning. Results in terms of outlet composition (mol fractions) of each stable species measured are shown in Fig. 8, compared to equilibrium predictions.

As all the mixtures were fuel-rich with respect to R2 (total oxidation), O_2 was always completely consumed after ignition, accordingly to the thermodynamic equilibrium that predicts total consumption of oxygen at every temperature. Increasing the O_2 concentration (higher Λ), shifts the products toward a higher presence of total oxidation species, H_2O and CO_2. In fact, equilibrium shows an increase of CO_2 and H_2O with a higher amount of oxygen in the feed, at every temperature. In the mid-temperature zone also, CO and H_2 concentrations are higher than those measured with CPO-stoichiometric O_2 ($\Lambda = 0.25$), both in the experimental and in the equilibrium profiles, because in the adiabatic reactor the heat release is higher with higher oxygen content and this supports a higher methane conversion, thus, a higher amount of products as well. Nonetheless, the real syngas selectivity, as shown in Fig. 9, will be lower with more CH_4 in the feed (lower Λ). At the highest T, the trend is the opposite, as expected from mechanistic considerations, and the H_2 and CO obtained at $\Lambda = 0.25$ are maxima.

The catalytic role of CeO_2 doping is evident in lowering the ignition temperature from approx. 450 °C to 390 °C, i.e., about 60 °C lower. It is important to notice, that the stoichiometry does not influence the ignition temperature, which is the same for the three feed mixtures used. The low temperature light off of the catalyst occurs because CeO_2 induces a modification of the support surface, with more lattice vacancies, which increases the oxygen mobility and enhances the reducibility of Rh [15]. As confirmed by the characterization analyses, the metal dispersion of the ceria–zirconia sample is about twice that of zirconia supported one. Furthermore, we showed that repeated cycles of reduction and oxidation further increase the dispersion when ceria is present, while the effect is very limited when Rh is supported on zirconia only. This means that more active sites are available for the reactant to adsorb, triggering the reaction at lower temperatures. On the other hand, the higher Rh dispersion is responsible for the higher methane conversion. For example, at $\Lambda = 0.30$, right after ignition, methane conversion is 51% for ZrO_2 and 59% for ZrO_2–CeO_2, despite the ignition temperature of ZrO_2–CeO_2 is lower. However, this is only partly due to an increase of active sites available for the total oxidation reaction, since O_2 concentration over the catalyst is negligible in most of the reactor length [62], due to a diffusion limited regime for oxygen [68]. In fact, Eriksson [26] also notices that the increase of Rh loading, from 0.5% to 2%, has a minor role on methane conversion. This observation is consistent with the diffusive regime condition, in which most of the Rh sites are unused. The effect of CeO_2 doping is to enhance the steam reforming reaction, because methane and steam adsorb on two different sites; methane is dissociatively adsorbed on the Rh sites while steam dissociatively adsorb on the support site to give gaseous H_2 and adsorbed O atoms (R5) [31]. This is why an inert support is not so effective in catalyzing the CPO reaction. Moreover, the support may contribute in retarding the carbon deposition. In our experiments, unexpectedly, at the

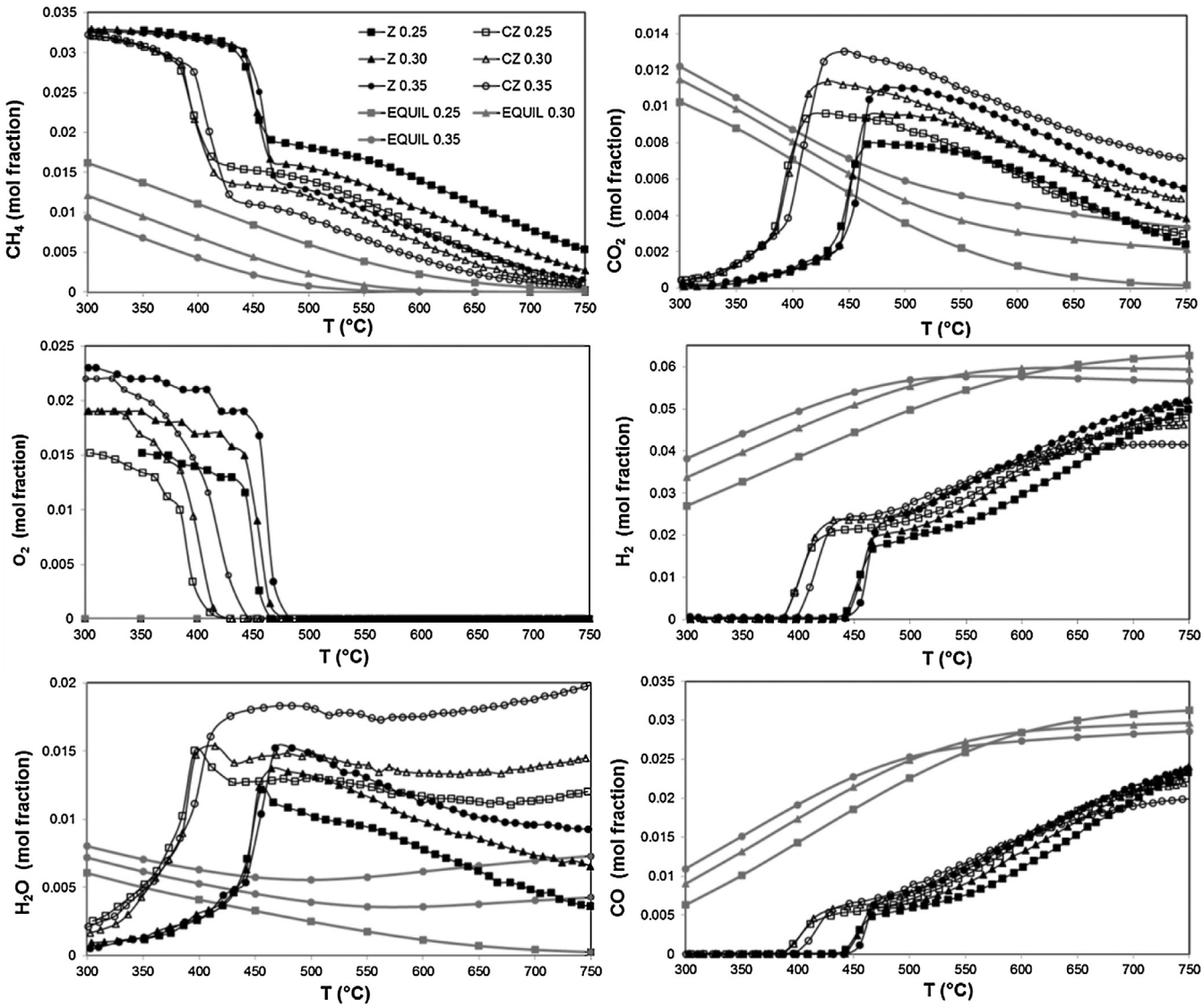

Fig. 8. Experimental (black) and equilibrium (gray) species molar fractions at the reactor outlet, varying the inlet temperature, for Rh/ZrO_2 and Rh/CeO_2–ZrO_2 catalysts, with $\Lambda = 0.25, 0.30, 0.35$.

highest T there are different behaviors for total and partial oxidation species. H_2O and CO_2 are higher with ZrO_2–CeO_2 than in the simple ZrO_2, for all the temperatures investigated. Consistently, lower yields of CO and particularly of H_2, is observed at increasing temperature. This was initially attributed to incipient carbon deposition, leading to lower catalyst activity. The bend in the production of syngas indeed occurs above 500 °C, where carbon is more likely to form [69]. The calculated carbon balance was between 98 and 101% for the Z sample and between 95 and 103% for the CZ sample. A carbon balance of $100 \pm 5\%$ is usually considered satisfactory and within the experimental error, but due to the experimental uncertainty the carbon deposition cannot be ruled out based solely on the C balance. Despite ceria is known to be beneficial for carbon deposition, the effective composition of the support has to be finely tuned to optimize the anticoking properties and the stability [30]. In order to confirm this hypothesis, a serie of tests was run keeping the catalyst at 730 °C for 6 h ($\Lambda = 0.25$). At the end of the prolongued test, air was fed to the reactor, the temperature was ramped from 300 to 750 °C and the outlet gas composition monitored for the possible formation of CO_2. None of the 4 samples tested (the 2 calcined in air and the 2 reduced ones) showed any development of CO_2. Carbon deposition is therefore, excluded as a cause for the change in the selectivity. In contrast, a likely explanation is that ceria is exhibiting its well known oxygen storage and release properties and reacts with CO and H_2 according to the following reactions:

$$2CeO_2 + CO \Leftrightarrow Ce_2O_3 + CO_2 \quad \text{(R9)}$$

$$2CeO_2 + H_2 \Leftrightarrow Ce_2O_3 + H_2O \quad \text{(R10)}$$

Both (R9) and (R10) are endothermic reactions, and are therefore, favored at high temperature. Furthermore, the presence of large amounts of CO and H_2 along most of the reactor length and the rich conditions created above 600 °C, also pushes the reaction toward the products. In addition, the TPR analyses show that the support is reduced above 500–550 °C, which matches fairly well with the temperature zone where the selectivity bend occur. Besides Reactions (R9) and (R10), the RWGS reaction could also be occurring, catalyzed by ceria, consuming hydrogen and CO_2 and forming CO and H_2O. Indeed, the bend of the H_2 curve is more marked than that on CO. Likely, all (R9), (R10) and RWGS reaction are occurring at the same time at temperatures above 600 °C.

It might appear counterintuitive that the experimental trends of CO_2 and H_2O cross the respective predicted equilibrium trends. In the case of a single simple reaction (e.g., R_1: $A = B$) that reaches the

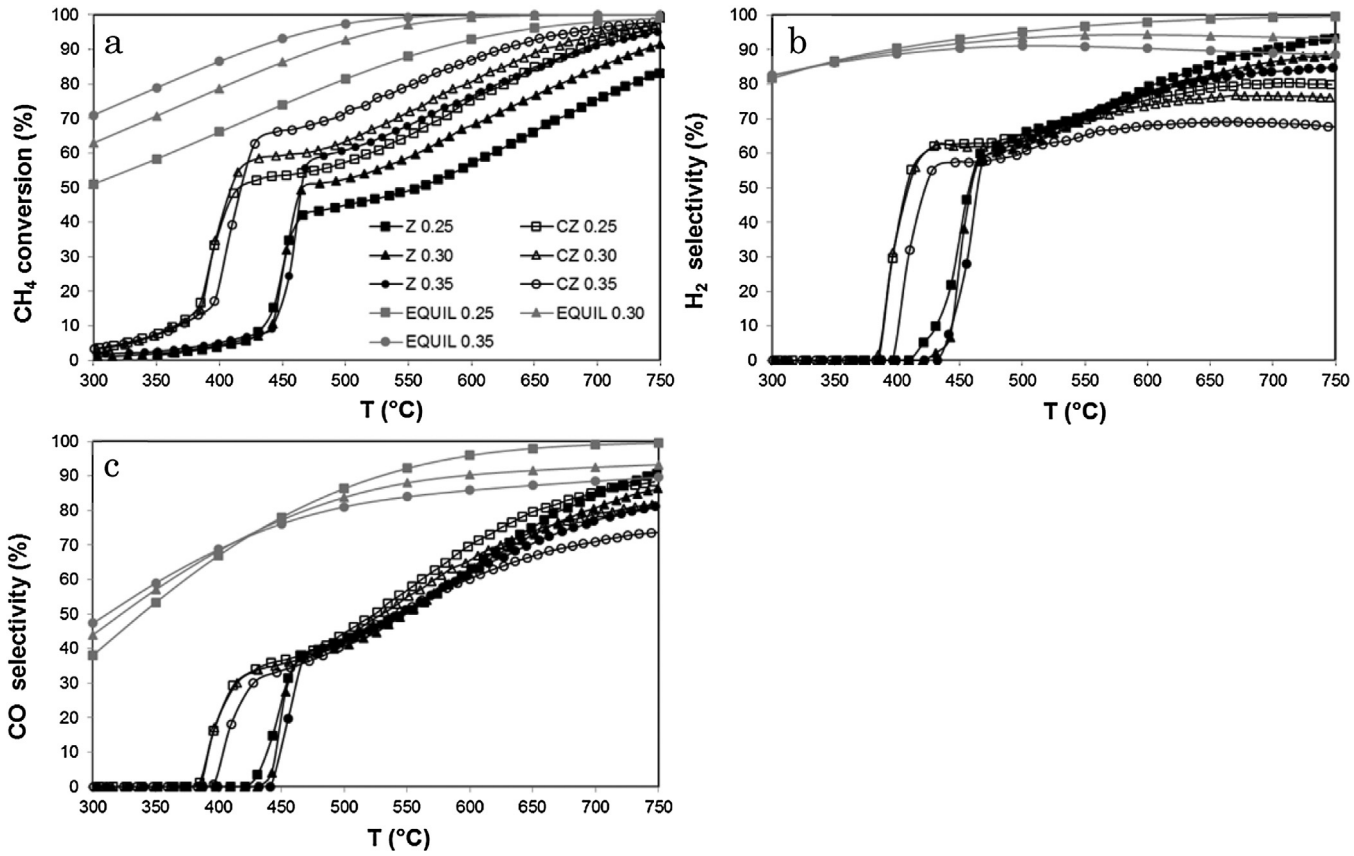

Fig. 9. Methane conversion (a) and H_2 and CO selectivity, (b) and (c), varying the inlet temperature. Experimental data for Rh/ZrO_2 (black, solid) and $Rh/CeO_2–ZrO_2$ (black, empty) catalysts, and equilibrium values (gray), with $\Lambda = 0.25–0.30–0.35$.

equilibrium, it is indeed, impossible for *B* molar fraction to cross the predicted equilibrium curve. However, in the case of, for example, two consecutive reactions, such as R_1 above and R_2: $B = C$, where the product *B* of R_1 becomes the reactant of R_2, the molar fraction of the specie *B* can become higher than the equilibrium value. This would happen if R1 reaches the equilibrium, but R_2 does not. This is exactly what happens in our systems, where *B* is either CO_2 or H_2O that are formed in a combustion step that reaches equilibrium, while the subsequent reforming reactions do not. Indeed, both CO_2 and H_2O molar fractions remain below the equilibrium values until H_2 and CO are formed, and cross the equilibrium after the reforming starts. This indicates that the global reaction is under kinetic control and has not yet reached the equilibrium state. That is also confirmed from the trends of the CH_4 molar fractions, which only approach the equilibrium values at the highest temperatures investigated.

We compared both catalysts at different CH_4/O_2 ratio in Fig. 9 in terms of CH_4 conversion and selectivity to CO and H_2. Fig. 9a shows that CH_4 conversion on 0.5 wt% Rh/ZrO_2 at 750 °C is above 80%, while it goes beyond 95% on 0.5 wt% $Rh/CeO_2–ZrO_2$. In Fig. 9, H_2 and CO selectivity are also shown. S_{H2} is 60% right after the ignition, and increases further up to 90% for Mix1 over Rh/ZrO_2, while it is much less for $Rh/Ce–ZrO_2$, likely because of the concurrent reduction of ceria, according to (R9) and (R10). S_{CO} sweeps from 30%, after ignition, to 70–90%, depending on the amount of O_2 in the feedstock. Syngas formation does not start until ignition. It must be inferred that in the low conversion region methane converts preferably to H_2O and CO_2, since there is abundant oxygen available for the total combustion.

As already pointed out above, the selectivity to syngas is higher at the CH_4 richer stoichiometries, at any temperature, but the absolute amount of syngas is higher with higher content of O_2. Fig. 9 also reports the expected performance, would the equilibrium be achieved. Significant CH_4 conversion is expected at temperature much lower than the experimental ignition, being already >50% at 300 °C, for any feed mixture. It approaches 100% above 600 °C for $\Lambda \geq 0.30$, and at 750 °C for $\Lambda = 0.25$. Noticeably, even if the reactants ratio allowed the full consumption of methane, this does not occur at low temperature, where some unreacted methane has to be expected among the products. The experimental conversions gradually approach the equilibrium, as the temperature rises, and are likely to reach it with higher contact times. Indeed, when the temperature increases, the gas velocity becomes higher, thus, decreasing the actual contact time, even at a fixed space velocity (which is calculated at 20 °C). Conversely, the contact time increases when the space velocity becomes lower, allowing the reaction to get closer to the equilibrium concentrations. In other words, the contact time is not the same during a heating cycle, but it becomes progressively shorter with increasing temperature. The $Rh/Ce–ZrO_2$ support is particularly effective in catalyzing the reactions, but either the short contact time and/or some transport limitations at higher temperature prevent the achievement of the equilibrium.

Note that CH_4 conversion due to total oxidation alone is 25%, 30% and 35% for $\Lambda = 0.25$, 0.30, 0.35. In the equilibrium predictions, Fig. 9a, we get twice as much already at 300 °C, and even more, raising the temperature. Thus, the most stable composition of such a reacting mixture always implies the presence of some partial oxidation species, in larger amount with increasing temperature. According to equilibrium, at 300 °C the H atoms from the reacted CH_4 must distribute 80% in H_2 and 20% in H_2O (Fig. 9), while the C atoms distribute almost equally between CO and CO_2 (Fig. 9c).

Table 7
Specific catalytic activity of our samples (*), compared to the literature. *m*- and *t*- stand for monoclinic and tetragonal ZrO_2. Unless otherwise indicated, all the comparisons are with Rh catalysts on zirconia or mixed ceria–zirconia supports.

Support/ref.	Ref.	% Metal	m_{cat} (g)	% CH_4	WHSV (Nl/kg_{cat} h)	T (°C)	X_{CH4}	mol_{CH4}/g_{met} h
*$Ce_{16}Zr_{84}O_2$ @ 800 °C		0.50%	0.126	3.3%	1.22E+06	800	0.99	327
*$Ce_{16}Zr_{84}O_2$ @ 600 °C		0.50%	0.126	3.3%	1.22E+06	600	0.77	255
$Ce_{0.5}Zr_{0.5}O_2$	[32]	1.00%	0.005	28.6%	4.20E+03	600	0.50	148
$Ce_{16}Zr_{84}O_2$ (Pt)	[46]	1.50%	0.020	66.7%	3.00E+05	800	0.24	131
*m-ZrO_2		0.50%	0.133	3.3%	1.16E+06	800	0.89	280
m-ZrO_2	[70]	0.39%	0.010	2.0%	9.00E+05	800	0.10	19
t-ZrO_2	[70]	0.50%	0.010	2.0%	9.00E+05	800	0.95	140
m-ZrO_2	[35]	0.50%	0.006	4.0%	1.10E+06	800	0.65	234
m-ZrO_2 (Pt)	[46]	1.50%	0.020	66.7%	3.00E+05	800	0.23	126

At 750 °C the selectivity to syngas is 100% for $\Lambda = 0.25$, because the reactants ratio is stoichiometric for the partial oxidation reaction, R1, and at high T the most stable species are H_2 and CO. With more O_2 in the feed, $\Lambda = 0.30$ and 0.35 some H_2O and CO_2 must be expected in the products. In such conditions, water gas shift (R4) equilibrium holds, supporting the reverse reaction at high temperature, being the reaction slightly exothermic. Hence, if CO is monotonously increasing with T, selectivity to H_2 shows a maximum, to follow the equilibrium criteria.

It is interesting to note that the combination of metal and support is crucial in determining the activity and selectivity of the catalyst. In a previous work [43], we tested ruthenium impregnated on different supports, for the same reaction and at the same conditions. The very same MEL Chemicals mixture of ceria and zirconia was used, but the catalyst activity was rather different compared to the one obtained with Rh. In particular, only 35% CH_4 conversion was reached at 700 °C and up to 680 °C, CO_2 was the main product. Only above that temperature CO and H_2 were produced in considerable amounts. Furthermore, the catalyst did not need any conditioning, but showed stable behavior since the first run.

In order to compare our results with other works in the literature, a specific activity was calculated for our samples and for some references, as reported in Table 7. We define as specific activity the moles of methane converted in an hour, at a given temperature, scaled on the mass of active metal. The specific activity is proportional to the turn over frequency (TOF), with the exception that the whole amount of metal on the catalyst sample is considered, instead than the fraction that is available for the reaction. In order to calculate the TOF, the metal dispersion is necessary and this information was not always available in the references considered. The values reported in Table 4 were measured on samples whose surface structure approximates the one of the tested catalyst, but might be different due to the mismatch of the redox conditions during the CPO and TPR/TPO tests. Still, retrieving all the information required to make a consistent comparison could be difficult, due to the great variability of the experimental conditions and of the materials used in different works. Further, it should be observed that powders are used in all the references considered, while in our work the catalyst was supported on a monolith. According to the calculated values, our catalysts on monolith result in a higher specific activity. Both the Z and the CZ samples show the highest conversion at the considered temperatures in every case. It is also remarkable that the above statement stands regardless of the support or even the type of active metal.

The performance of the Rh/ZrO_2 sample are partly in contrast with the findings of Campa et al. [70], who report very poor activity for a 0.4% Rh/ZrO_2 sample. In the cited work, the effect of the crystalline structure of the support is highlighted, and it is shown that the tetragonal zirconia provides much higher activity compared to the monoclinic phase. For the monoclinic sample, which is the structure detected on our catalyst, a poor conversion (about 20%) is reported, even at temperature in excess of 700 °C, while our sample shows conversion above 80%.

The number of references considered is quite limited, but the data provided suggest that the ratio between the reactants flow rate, the amount of catalyst and the reactor volume was not optimal. It appears that monoliths allow to better exploit the powder catalyst. Likely, combination of exo- and endothermic reactions determine unfavorable local temperature in powders.

4. Conclusions

Methane partial oxidation on Rh catalysts supported on ZrO_2 and $Ce_{0.16}Zr_{0.84}O_2$ was studied experimentally. In addition to temperature, the feed composition was varied, always on the CH_4 rich side. We measured by XRD a structural effect of doping with CeO_2, which preserved the tetragonal structure from reverting to monoclinic. Activity measurements showed that ZrO_2 required a rather long initial conditioning, i.e., 11 temperature cycles to achieve stable performances, while CeO_2–ZrO_2 does not; the latter reaches its stable activity after just few temperature cycles. TPR/TPO and chemisorption analysis showed that the conditioning procedure leads to changes in the metal structure, with the particles size decreasing and a consequent increase of the dispersion. The phenomenon is caused by alternating oxidizing and reducing conditions occurring during the CPO tests.

Adding ceria to the support lowers the catalyst ignition temperature by approx. 60 °C, and, already right after light off, the resulting catalyst is more active, e.g., plus 8% conversion for the $\Lambda = 0.30$ stoichiometry. CH_4 conversion at 750 °C is above 80% on 0.5 wt% Rh/ZrO_2 while it goes beyond 95% on 0.5 wt% Rh/CeO_2–ZrO_2. Measurements are always below the equilibrium, though quite close at the highest temperature, also because of the high GHSV used, keeping the process under kinetic control to highlight catalysts differences.

Syngas selectivity, after light off (at different temperatures), is comparable in the two catalysts and it is higher for the CH_4 richer stoichiometry, according to the thermodynamic equilibrium, even if the amount of H_2 and CO produced is higher at the higher O_2 content. Above 500 °C, the higher syngas selectivity of ZrO_2 is due to the OSC of ceria, which, when incorporated in the CZ sample, works as an oxygen buffer and reacts according to Reactions (R9) and (R10), consuming CO and H_2 and forming CO_2 and H_2O. Furthermore, ceria also might catalyze the RWGS reaction, which contributes in changing the product distribution. The selectivity to syngas is higher at lower O_2/CH_4 ratio, at any temperature, but the absolute amount of syngas is higher with more O_2, because of the higher methane conversion and the related higher heat release.

Although measurements are not spatially resolved along the catalyst, results clearly indicate that reforming reactions activate only after CH_4 total oxidation has completed, with the available O_2, meaning that both the samples tested follow the indirect mechanism.

References

[1] S.C. Tsang, J.B. Claridge, M.L.H. Green, Catal. Today 23 (1995) 3–15.
[2] D.A. Hickman, L.D. Schmidt, J. Catal. 138 (1992) 267–282.
[3] P.M. Torniainen, X. Chu, L.D. Schmidt, J. Catal. 146 (1994) 1–10.
[4] BP Statistical Review of World Energy June 2014, in, <http://www.bp.com/en/global/corporate/about-bp/energy-economics/statistical-review-of-world-energy.html> (2014).
[5] G. van Rossum, B. Potic, S.R.A. Kersten, W.P.M. van Swaaij, Catal. Today 145 (2009) 10–18.
[6] H. Jahangiri, J. Bennett, P. Mahjoubi, K. Wilson, S. Gu, Catal. Sci. Technol. 4 (2014) 2210–2229.
[7] A.Y. Krylova, Solid Fuel Chem. 48 (2014) 22–35.
[8] A. Lappas, E. Heracleous, Handbook of Biofuels Production, in: R. Luque, J. Campelo, J. Clark (Eds.), Woodhead Publishing, 2011, pp. 493–529.
[9] D. Dalle Nogare, P. Baggio, C. Tomasi, L. Mutri, P. Canu, Chem. Eng. Sci. 62 (2007) 5418–5424.
[10] A. Jess, R. Popp, K. Hedden, Appl. Catal. A-Gen. 186 (1999) 321–342.
[11] X.-F. Ye, S.R. Wang, J. Zhou, F.R. Zeng, H.W. Nie, T.L. Wen, J. Power Sources 195 (2010) 7264–7267.
[12] R. Lanza, J.A. Velasco, S.G. Jaras, Catal. 23, R. Soc. Chem. (2011) 50–95.
[13] T.V. Choudhary, V.R. Choudhary, Angew. Chem. Int. Ed. (English) 47 (2008) 1828–1847.
[14] P.D.F. Vernon, M.L.H. Green, A.K. Cheetham, A.T. Ashcroft, Catal. Today 13 (1992) 417–426.
[15] J. Zhou, K. Wu, W. Wang, Y. Han, Z. Xu, H. Wan, S. Zheng, D. Zhu, Appl. Catal. B-Environ. 162 (2015) 85–92.
[16] N. Kamiuchi, M. Haneda, M. Ozawa, Catal. Today Part A 241 (2015) 100–106.
[17] T.A. Maia, E.M. Assaf, R. Soc, Chem. Adv. 4 (2014) 31142–31154.
[18] H.-S. Roh, I.-H. Eum, D.-W. Jeong, Renew. Energy 42 (2012) 212–216.
[19] R. Horn, K.A. Williams, N.J. Degenstein, A. Bitsch-Larsen, D. Dalle Nogare, S.A. Tupy, L.D. Schmidt, J. Catal. 249 (2007) 380–393.
[20] R. Horn, K.A. Williams, N.J. Degenstein, L.D. Schmidt, J. Catal. 242 (2006) 92–102.
[21] Z. Hu, F.M. Allen, C.Z. Wan, R.M. Heck, J.J. Steger, R.E. Lakis, C.E. Lyman, J. Catal. 174 (1998) 13–21.
[22] H.C. Yao, S. Japar, M. Shelef, J. Catal. 50 (1977) 407.
[23] H.C. Yao, H.K. Stepien, H.S. Gandhi, J. Catal. 61 (1980) 547–550.
[24] R. Burch, P.K. Loader, Appl. Catal. A-Gen. 143 (1996) 317–335.
[25] G. Pecchi, P. Reyes, R. Gómez, T. López, J.L.G. Fierro, Appl. Catal. B-Environ. 17 (1998) L7–L13.
[26] S. Eriksson, M. Wolf, A. Schneider, J. Mantzaras, F. Raimondi, M. Boutonnet, S. Järås, Catal. Today 117 (2006) 447–453.
[27] J.A. Wang, T. López, X. Bokhimi, O. Novaro, J. Mol. Catal. A-Chem. 239 (2005) 249–256.
[28] S. Eriksson, S. Rojas, M. Boutonnet, J.L.G. Fierro, Appl. Catal. A-Gen. 326 (2007) 8–16.
[29] S. Boullosa-Eiras, T. Zhao, D. Chen, A. Holmen, Catal. Today 171 (2011) 104–115.
[30] F.A. Silva, K.A. Resende, A.M. da Silva, K.R. de Souza, L.V. Mattos, M. Montes, E.F. Souza-Aguiar, F.B. Noronha, C.E. Hori, Catal. Today 180 (2012) 111–116.
[31] M.H. Halabi, M.H.J.M. de Croon, J. van der Schaaf, P.D. Cobden, J.C. Schouten, Appl. Catal. A-Gen. 389 (2010) 68–79.
[32] A.J. Santis-Alvarez, R. Büchel, N. Hild, W.J. Stark, D. Poulikakos, Appl. Catal. A-Gen. 469 (2014) 275–283.
[33] A. Beretta, T. Bruno, G. Groppi, I. Tavazzi, P. Forzatti, Appl. Catal. B-Environ. 70 (2007) 515.
[34] A. Beretta, A. Donazzi, G. Groppi, P. Forzatti, V. Dal Santo, L. Sordelli, V. De Grandi, R. Psaro, Appl. Catal. B-Environ. 83 (2008) 96.
[35] T. Bruno, A. Beretta, G. Groppi, M. Roderi, P. Forzatti, Catal. Today 99 (2005) 89–98.
[36] K.-i Tanaka, Catal. Today 154 (2010) 105–112.
[37] K.-i Tanaka, H. He, Catal. Today 201 (2013) 2–6.
[38] J.M. Gatica, R.T. Baker, P. Fornasiero, S. Bernal, G. Blanco, J. Kašpar, J. Phys. Chem. B 104 (2000) 4667–4672.
[39] X. Karatzas, K. Jansson, A. Gonzalez, J. Dawody, L.J. Pettersson, Appl. Catal. B 106 (2011) 476–487.
[40] S. Boullosa-Eiras, T. Zhao, E. Vanhaecke, D. Chen, A. Holmen, Catal. Today 178 (2011) 12–24.
[41] X. Karatzas, K. Jansson, J. Dawody, R. Lanza, L.J. Pettersson, Catal. Today 175 (2011) 515–523.
[42] A. Ishikawa, E. Iglesia, J. Catal. 252 (2007) 49–56.
[43] R. Lanza, S.G. Järås, P. Canu, Appl. Catal. A-Gen. 325 (2007) 57–67.
[44] D.G. Goodwin, Cantera: Object-Oriented Software for Reacting Flows Technical Report, Institute of Technology, California, 2002.
[45] C.E. Hori, H. Permana, K.Y.S. Ng, A. Brenner, K. More, K.M. Rahmoeller, D. Belton, Appl. Catal. B-Environ. 16 (1998) 105–117.
[46] F.B. Passos, E.R. de Oliveira, L.V. Mattos, F.B. Noronha, Catal. Today 101 (2005) 23–30.
[47] M. Pudukudy, Z. Yaakob, Pharma Chem. 6 (2014) 188–216.
[48] M. Pudukudy, Z. Yaakob, Pharma Chem. 6 (2014) 224–240.
[49] M. Shen, L. Lv, J. Wang, J. Zhu, Y. Huang, J. Wang, Chem. Eng. J. 255 (2014) 40–48.
[50] H.-C. Yang, M.-W. Lee, H.-S. Hwang, J.-K. Moon, D.-Y. Chung, J. Rare Earth. 32 (2014) 831–836.
[51] W.-P. Dow, Y.-P. Wang, T.-J. Huang, J. Catal. 160 (1996) 155–170.
[52] A. Holmgren, B. Andersson, Oxygen Storage J. Catal. 178 (1998) 14–25.
[53] J.L. Ayastuy, M.P. González-Marcos, A. Gil-Rodríguez, J.R. González-Velasco, M.A. Gutiérrez-Ortiz, Catal. Today 116 (2006) 391–399.
[54] E. Bekyarova, P. Fornasiero, J. Kašpar, M. Graziani, Catal. Today 45 (1998) 179–183.
[55] G. Balducci, P. Fornasiero, R. Di Monte, J. Kaspar, S. Meriani, M. Graziani, Catal. Lett. 33 (1995) 193–200.
[56] P. Fornasiero, R. Dimonte, G.R. Rao, J. Kaspar, S. Meriani, A. Trovarelli, M. Graziani, J. Catal. 151 (1995) 167–168.
[57] W.K. Jóźwiak, React. Kinet. Catal. Lett. 30 (1986) 345–351.
[58] M.Z. Granlund, K. Jansson, M. Nilsson, J. Dawody, L.J. Pettersson, Appl. Catal. B-Environ. 154–155 (2014) 386–394.
[59] M.D. Salazar-Villalpando, D.A. Berry, T.H. Gardner, Int. J. Hydrogen Energy 33 (2008) 2695–2703.
[60] J.C. Vis, H.F.J. van 't Blik, T. Huizinga, J. van Grondelle, R. Prins, J. Catalysis, (1985) 333–345.
[61] L. Cao, L. Pan, C. Ni, Z. Yuan, S. Wang, Fuel Process. Technol. 91 (2010) 306–312.
[62] D. Dalle Nogare, N.J. Degenstein, R. Horn, P. Canu, L.D. Schmidt, J. Catal. 258 (2008) 131–142.
[63] B. Kimmerle, J.-D. Grunwaldt, A. Baiker, P. Glatzel, P. Boye, S. Stephan, C.G. Schroer, J. Phys. Chem. C 113 (2009) 3037–3040.
[64] J.-D. Grunwaldt, B. Kimmerle, A. Baiker, P. Boye, C.G. Schroer, P. Glatzel, C.N. Borca, F. Beckmann, Catal. Today 145 (2009) 267–278.
[65] B. Christian Enger, R. Lødeng, A. Holmen, Appl. Catal. A-Gen. 346 (2008) 1–27.
[66] A. Bitsch-Larsen, R. Horn, L.D. Schmidt, Appl. Catal. A-Gen. 348 (2008) 165–172.
[67] T. Liu, C. Snyder, G. Veser, Ind. Eng. Chem. Res. 46 (2007) 9045–9052.
[68] M. Maestri, A. Beretta, G. Groppi, E. Tronconi, P. Forzatti, Catal. Today 105 (2005) 709–717.
[69] D. Wayne Goodman, T.V. Choudhary, Catal.: R. Soc. Chem. 19 (2006) 164–183.
[70] M.C. Campa, G. Ferraris, D. Gazzoli, I. Pettiti, D. Pietrogiacomi, Appl. Catal. B-Environ. 142–143 (2013) 423–431.